

Ultrafast dynamics of photoinduced terahertz electron-hole plasma waves in semiconductor junctions

Junheng Pan ¹, Sheng Liu ^{1,2,3,*} and Jau Tang ^{2,†}

¹Key Laboratory of Hydropower Transients of Ministry of Education, School of Power and Mechanical Engineering, Wuhan University, Wuhan 430072, China

²Laboratory for Electronic Manufacturing and Packaging Integration, The Institute of Technological Sciences, Wuhan University, Wuhan 430072, China

³School of Microelectronics, Wuhan University, Wuhan 430072, China



(Received 21 October 2020; revised 23 June 2021; accepted 28 June 2021; published 20 July 2021)

The ultrafast transport processes of electrons and holes excited by femtosecond laser pulses are essential for a better understanding of carrier dynamics in semiconductors. Transient optical techniques are commonly used to investigate the carrier excitation and transport in these materials. Recently, ultrafast scanning electron microscopy has been employed to elucidate the ballistic dynamics of such hot carriers near a p - n junction. We provide here a model not only to explain the previously reported superfast expansion of electron-hole clouds but also to predict plasma wave behavior at high laser fluences. In addition to a bipolar junction, we also investigate the well structure of a p - n - p junction sandwiched by insulating layers. By confining hot carriers inside junctions, these carriers begin to oscillate as a result of Coulomb interactions among carriers and with the intrinsic field at the depletion zone, leading to the occurrence of terahertz-scale plasma waves for potential applications as pulsed terahertz light sources.

DOI: [10.1103/PhysRevB.104.045309](https://doi.org/10.1103/PhysRevB.104.045309)

I. INTRODUCTION

With the development of information technology, fast processing speed at greater efficiencies is required for high-performance electronic devices with great speeds. The ultrafast dynamics of the charge carriers of materials play a crucial role in these critical properties. The time scale of charge carrier dynamics covers a wide range from nanoseconds to femtoseconds, which makes their detection very difficult. The development of ultrashort pulse laser technology has provided researchers with powerful tools to investigate the ultrafast carrier dynamics of materials so that applications could be made. Ultrafast spectroscopy techniques, including time-resolved photoluminescence [1–4] spectroscopy and transient absorption [5–9] spectroscopy, make it possible to measure charge carrier dynamics at a high time resolution. However, ultrafast spectroscopy indirectly infers carrier dynamics by observing changes in the optical properties of materials. Pump-probe microscopy has become an effective method for characterizing charge carrier dynamics [10–16]. However, due to the diffraction limit of light in these optical methods, challenges still remain for observing ultrafast carrier dynamics at a much higher spatial and temporal resolution. In recent years, ultrafast scanning electron microscopy (USEM) has been developed to provide direct visualization of carrier processes with high precision, which combines the femtosec-

ond temporal resolution of ultrafast lasers with the nanometer spatial resolution of scanning electron microscopy [17–21].

Although it is possible to use USEM to observe the ultrafast carrier dynamics of materials, better physical understanding and theoretical modeling still remain a challenge. For example, the Monte Carlo method, used to explain carrier dynamics measurements from ultrafast spectroscopy [22], is an empirical approach with multiple parameters and is not universally applicable. The other method using the first-principles approach does not require fitting parameters and has higher accuracy. However, this approach is used to model ultrafast carrier dynamics of a very small ensemble of particles at very short time scales [23,24]. Nevertheless, it is still a challenging task to use the first-principles approach to simulate the charge carrier dynamics from femtoseconds to nanoseconds for an ensemble of microns in size. The purpose of this paper is to provide model simulations for visualizing a micron-sized electron-hole cloud to evolve after a femtosecond laser excitation of semiconductor junctions.

In our previous work [18], we used four-dimensional scanning electron microscopy to investigate ultrafast charge carrier dynamics in semiconductors with a nanometer spatial resolution and femtosecond temporal resolution. In that study, we and the coauthors investigated ultrafast charge separation of the photo-induced electrons and holes near a p - n junction. We observed the formation of two oppositely charged domains rapidly expanding away from the irradiated area at a speed much faster than simple carrier diffusion. To account for such behavior, we proposed a ballistic mechanism and a simplified model to qualitatively explain the charge separation and

* shengliu@whu.edu.cn

† jautang@yahoo.com

transport of carriers. In that model, we focused primarily on the rectification effects due to the ballistic motion of the hot carriers in the presence of the internal electric field inside the depletion zone near the junction. However, in that simplified model, we did not consider the Coulomb interactions among the carriers because such interactions are insignificant at a low laser fluence as used in the experiment. In this paper, we construct a more realistic theoretical model to include the Coulomb interactions among the charged carriers so that we can more precisely account for scenarios when the carrier density is sufficiently large at a high laser excitation. In addition, instead of assuming previously a vertical potential well inside the junction depletion zone, we consider here a more realistic electrical potential in the depletion zone where photoexcited electrons and holes can be accelerated or decelerated. Now with this more realistic model, we could investigate carrier dynamics in a bipolar semiconducting junction as well as a p - n - p triode sandwiched by insulating layers and the resultant interesting plasma wave phenomena.

A femtosecond laser with photon energy greater than the semiconductor bandgap has been commonly used to excite electrons from the valence band to the conduction band, leaving holes in the valence band. These charge carriers, in the presence of an external voltage bias, can form a transient current to induce terahertz electromagnetic (EM) radiation [25]. Similar processes can also occur on the surface of semiconductors due to differences in the photo-induced charge density between the surface and the bulk [26–28]. It would be interesting to know what will happen if one takes advantage of the internal electric field of the depletion zone between the p - and n -type regions. Our calculations in this paper show that electron-hole plasma waves could occur in a p - n or p - n - p junction. Such plasma wave phenomena become more prominent at a high laser fluence as the Coulomb interactions become stronger at a higher carrier density. Moreover, such plasma oscillations are more effective for a p - n - p triode junction sandwiched by two insulating layers due to carrier confinement within the boundaries. The frequencies of the plasma cloud oscillations are found to be in the terahertz range, indicating potential applications as a terahertz light source.

II. MODEL AND SIMULATION METHOD

According to our previous work [18], to explain the very fast expansion of an electron-hole cloud after femtosecond laser excitation, we considered a ballistic model to describe the charge separation and hot carrier transport. Although such a model is sufficient for a qualitative explanation for the observed carrier dynamics at low fluence, it could not account for plasma wave behavior at larger fluence when the carrier density becomes higher. The main goal of this paper is to address such an issue and also to improve the modeling of the depletion zone potential well by replacing the vertical barrier by a more realistic physical model. In the improved model calculations, we consider a Newtonian ballistic motion for the hot electrons and holes in a force field consisting of intercarrier Coulomb interactions and depletion zone potential wells.

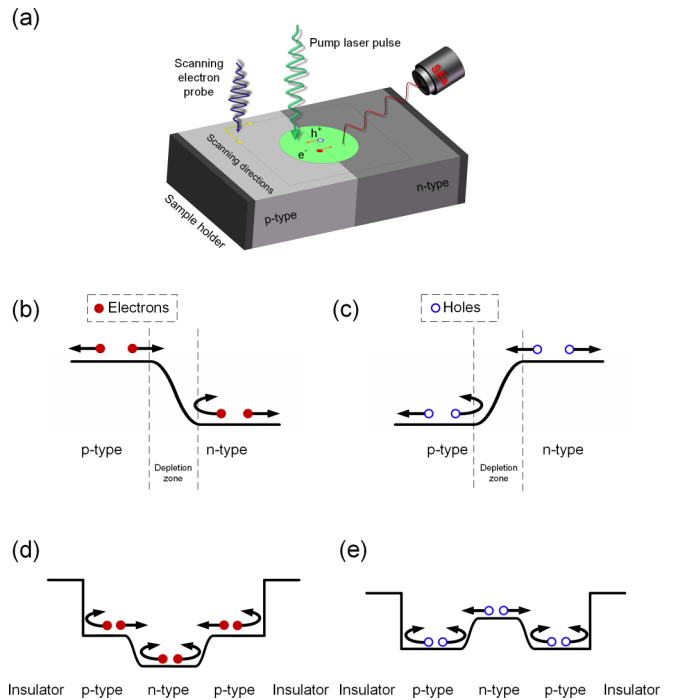


FIG. 1. Schematic diagram of photo-induced plasma waves near various types of semiconductor junctions. (a) Schematic diagram of the experimental setup of an ultrafast scanning electron microscope (USEM). The green domain represents the electron-hole cloud excitation on the surface near the p - n junction. A secondary electron (SE) detector measures the surface charge distribution. (b) and (c) Transport behavior of electrons (solid red spheres) and holes (hollow blue spheres) after photoexcitation on a bipolar p - n junction. (d) and (e) Movement of the excited carriers near the quantum-well junction composed of a p - n - p junction sandwiched by two insulating layers.

The schematic of the experimental setup for plasma wave excitation is shown in Fig. 1(a). The semiconductor junction contains a phosphorus-doped n -type silicon layer at a dopant concentration $1.0 \times 10^{14} \text{ cm}^{-3}$ and a boron-doped p -type silicon layer at a concentration of $1.0 \times 10^{19} \text{ cm}^{-3}$. At these dopant concentrations, the calculated electric potential of the depletion zone in the bipolar junction is estimated to be 0.77 V. Given femtosecond laser pulses (515 nm) are irradiated upon the surface of the semiconductor junction with a root mean square of $20 \mu\text{m}$ for the laser spot size. For simplicity, we assume that the p - and n -type silicon layers have the same amount of light absorption, resulting in an equal number of photo-induced electron-hole pairs in the p - and n -type regions. The carrier densities of the p -type ($\rho_p^{e,h}$) and n -type ($\rho_n^{e,h}$) obey a Gaussian spatial distribution at $t = 0$ because the intensity profile of the laser beam has a Gaussian shape. We also assume that the photo-induced hot carriers are at thermal equilibrium initially right after laser excitation. The initial velocities of the electron (f_e) and hole (f_h) follow the Maxwell-Boltzmann velocity distribution. Figures 1(b) and 1(d) represent the electron transport process on each side of the junction. Figures 1(c) and 1(e) represent the motion of holes that are positively charged. Taking the p type as an example, if the initial moving direction of the electron is from the n - to the p -type region, electrons will be bounced back

due to the influence of the junction barrier. For the triode sandwiched by two insulating layers, electrons and holes are confined within the region between the outside layers because these carriers cannot tunnel through the large barrier.

In model simulations, we consider the ballistic motion of the hot carriers in the presence of the depletion zone potential and the Coulomb forces between charges. Interparticle Coulomb forces and the electric field inside the depletion zone play an important role in the push-and-pull mechanism to cause oscillations of the photo-induced electron and hole clouds, which manifest themselves as charge density waves, or called plasma waves.

The initial normalized probability densities of electrons and holes in the p - and n -type regions are given by the following Gaussian spatial distributions:

$$\rho_{e,h}^p(x, y) = \frac{1}{2} \frac{1}{2\pi\sigma^2} \exp\left(-\frac{x^2 + y^2}{2\sigma^2}\right) \eta(-x), \quad (1)$$

$$\rho_{e,h}^n(x, y) = \frac{1}{2} \frac{1}{2\pi\sigma^2} \exp\left(-\frac{x^2 + y^2}{2\sigma^2}\right) \eta(x), \quad (2)$$

where η is the Heaviside step function, and σ is the laser spot size. We employed the finite element method to numerically calculate the time evolution of hot carriers according to ballistic Newtonian mechanics with a grid length of 1 μm . According to the Maxwell-Boltzmann distribution, the velocities of the electrons and holes are given by

$$f_e(v_x, v_y) = \frac{m_e^*}{2\pi K_B T} \exp\left(-\frac{v_x^2 + v_y^2}{2K_B T} m_e^*\right), \quad (3)$$

$$f_h(v_x, v_y) = \frac{m_h^*}{2\pi K_B T} \exp\left(-\frac{v_x^2 + v_y^2}{2K_B T} m_h^*\right), \quad (4)$$

where K_B is the Boltzmann constant, T is the temperature of the carriers, and v_x and v_y are the velocities of the carriers in the x and y directions, respectively. The effective mass of electrons and holes in silicon is provided by $m_e^* = 0.26m_e$ and $m_h^* = 0.386m_e$, respectively. The initial temperature of the carrier is estimated and assumed to be $\sim 10^4$ K. The average thermal velocities of electrons and holes are provided by

$$V_e = \sqrt{\frac{K_B T}{m_e^*}}, \quad (5)$$

$$V_h = \sqrt{\frac{K_B T}{m_h^*}}. \quad (6)$$

In the above simulations, we consider the carrier dynamics in two dimensions (2D) on the junction surface. At low fluence, when the carrier density is low, and the Coulomb interaction between the electron and hole clouds is insignificant, the trajectory calculation for each carrier is independent of others, and therefore, the computation time is not too time consuming. However, if one includes the Coulomb forces among carriers in the high fluence regime, the trajectory of each carrier becomes dependent on the position of all other carriers, and therefore, the computation time increases by several orders of magnitude; thus, the simulation task moves beyond the capability of a common laboratory workstation.

As a consequence, we can only simulate the one-dimensional (1D) case. For the 1D case, the probability densities of electrons and holes are given by

$$\rho_{e,h}(x) = \frac{1}{\sqrt{2\pi}\sigma} \exp\left(-\frac{x^2}{2\sigma^2}\right). \quad (7)$$

The velocity distributions of the electrons and holes are given by

$$f_e(v) = \frac{1}{\sqrt{2\pi}V_e} \exp\left(-\frac{v^2}{2V_e^2}\right), \quad (8)$$

$$f_h(v) = \frac{1}{\sqrt{2\pi}V_h} \exp\left(-\frac{v^2}{2V_h^2}\right). \quad (9)$$

After photoexcitation, the motion of hot electrons and holes is subject to the forces inside the depletion zone, the intercarrier Coulomb forces and the frictional damping forces. The accelerations of the k th electron and the k th hole, $a(x_{e,k})$ and $a(x_{h,k})$, respectively, consist of accelerations from three types of forces:

$$a(x_{e,k}) = \frac{F_D(x_{e,k})}{m_e^*} + a_C(x_{e,k}) - \frac{v_{e,k}}{\tau}, \quad (10)$$

$$a(x_{h,k}) = \frac{F_D(x_{h,k})}{m_h^*} + a_C(x_{h,k}) - \frac{v_{h,k}}{\tau}, \quad (11)$$

where $x_{e,k}$ and $x_{h,k}$ represent their respective positions. The first term on the right represents the acceleration due to the depletion zone force, the second terms $a_C(x_{e,k})$ and $a_C(x_{h,k})$ are the accelerations of the k th electron and the k th hole caused by intercarrier Coulomb forces, and the third terms are due to friction, where $v_{e,k}$ and $v_{h,k}$ are the velocities of the k th electron and the k th hole. The parameter τ is the frictional time constant. Based on preliminary experiments, this value is on the order of a few hundred picoseconds, and in our simulations, 1000 ps was used to more clearly illustrate the underdamped behavior. For the depletion zone force field [29], the distribution of the built-up electric field in the depletion zone and electric field force is provided by

$$E(x) = \begin{cases} -\frac{eN_a}{\epsilon_s}(x - x_p) & x_p \leq x \leq 0 \\ \frac{eN_d}{\epsilon_s}(x_n - x) & 0 \leq x \leq x_n \end{cases}, \quad (12)$$

$$F_D(x_{e,k}) = q_e E(x_{e,k}), \quad (13)$$

$$F_D(x_{h,k}) = q_h E(x_{h,k}), \quad (14)$$

where $E(x)$ is the electric field strength inside the space charge region, F_D is the depletion zone force, ϵ_s is the dielectric constant of silicon, N_a and N_d are the p - and n -type doping concentrations, respectively, and x_p and x_n are the boundaries of the space charge layer in the p and n regions, respectively. Because electrons and holes have opposite charges, $q_e = -q_h = -1.6 \times 10^{-19} \text{C}$. The accelerations for the carriers due to interparticle Coulomb interaction in the second term to the right of Eqs. (10) and (11) are based on Coulomb's

law:

$$\begin{aligned}
a_C(x_{e,k}) &= \frac{F_C^e(x_{e,k}) + F_C^h(x_{e,k})}{m_e^*} \\
&= \frac{\sum_{i=1}^w k_c \frac{q_e N_0 q_e R_e(x_i)}{(x_{e,k} - x_i)^2} \Delta x + \sum_{i=1}^w k_c \frac{q_e N_0 q_h R_h(x_i)}{(x_{e,k} - x_i)^2} \Delta x}{m_e^*} \\
&= \frac{k_c N_0 q_e^2}{m_e^*} \sum_{i=1}^w \frac{R_e(x_i) - R_h(x_i)}{(x_{e,k} - x_i)^2} \Delta x \\
&= \frac{k_c N_0 q_e^2}{m_e^*} \sum_{i=1}^w \frac{R(x_i)}{(x_{e,k} - x_i)^2} \Delta x \quad (x_{e,k} \neq x_i), \quad (15)
\end{aligned}$$

where $F_C^e(x_{e,k})$ and $F_C^h(x_{e,k})$ represent the Coulomb force between the k th electron and all other electrons and holes, respectively. The parameter k_c is the Coulomb constant. In our finite element method to numerically calculate the carrier trajectories, the spatial discretization is divided into w grid nodes with equal grid length $\Delta x = 0.6 \mu\text{m}$. The x_i represents the spatial position of the grid node. The $R_e(x_i)$ and $R_h(x_i)$ represent the charge density distribution of electrons and holes in space, respectively. So $R(x_i) = R_e(x_i) - R_h(x_i)$ represents the difference between the electron and hole charge densities. Here, N_0 is the initial number of hot electrons and holes in the system. Here, we define K as $k_c N_0 q_e^2 / m_e^*$ in Eq. (15), which is proportional to the number of hot carriers N_0 and the Coulomb constant k_c , and

$$N_0 = \frac{K m_e^*}{k_c q_e^2}. \quad (16)$$

For examples, $K = 20, 40, 60, 80, 100$, and 120 correspond to an initial number of carriers $N_0 = 2.06 \times 10^4, 4.11 \times 10^4, 6.17 \times 10^4, 8.22 \times 10^4, 1.03 \times 10^5$, and 1.23×10^5 in the 1D case, respectively. For the 2D case, the initial number of carriers is $4.23 \times 10^8, 1.69 \times 10^9, 3.80 \times 10^9, 6.76 \times 10^9, 1.06 \times 10^{10}$, and 1.52×10^{10} accordingly. This parameter plays an important role in controlling plasma wave behavior.

A similar analysis can be provided for the accelerations of holes caused by Coulomb forces. Therefore, one has

$$\begin{aligned}
a_C(x_{h,k}) &= \frac{F_C^e(x_{h,k}) + F_C^h(x_{h,k})}{m_h^*} \\
&= -\frac{k_c N_0 q_e^2}{m_h^*} \sum_{i=1}^w \frac{R(x_i)}{(x_{h,k} - x_i)^2} \Delta x \quad (x_{h,k} \neq x_i), \quad (17)
\end{aligned}$$

where $F_C^e(x_{h,k})$ and $F_C^h(x_{h,k})$ are the Coulomb forces between the k th hole and all other electrons and holes, respectively. According to Eqs. (15)–(17), we have

$$a_C(x_{e,k}) = K \sum_{i=1}^w \frac{R(x_i)}{(x_{e,k} - x_i)^2} \Delta x \quad (x_{e,k} \neq x_i), \quad (18)$$

$$a_C(x_{h,k}) = -K \sum_{i=1}^w \frac{R(x_i)}{(x_{h,k} - x_i)^2} \Delta x \frac{m_e^*}{m_h^*} \quad (x_{h,k} \neq x_i). \quad (19)$$

To avoid the singularity in Eqs. (18) and (19), $\delta = 0.1 \Delta x^2$ or $0.036 \mu\text{m}^2$ is introduced into the denominator. Equations (18) and (19) are further modified to

$$\begin{aligned}
a_C(x_{e,k}) &= K \sum_{i=1}^w \frac{R(x_i)(x_{e,k} - x_i)}{[(x_{e,k} - x_i)^2 + \delta]^{3/2}} \Delta x \quad (x_{e,k} \neq x_i), \quad (20) \\
a_C(x_{h,k}) &= -K \sum_{i=1}^w \frac{R(x_i)(x_{h,k} - x_i)}{[(x_{h,k} - x_i)^2 + \delta]^{3/2}} \Delta x \frac{m_e^*}{m_h^*} \quad (x_{h,k} \neq x_i). \quad (21)
\end{aligned}$$

The function $R(x_i; t)$ represents the difference between the electron and hole charge densities in space and time by integrating over the range of velocities for the distribution of net time-dependent charge carrier density:

$$R(x_i; t) = R_e(x_i; t) - R_h(x_i; t), \quad (22)$$

$$\begin{aligned}
R_e(x_i; t) &= \sum_k f_e[v_{e,k}(t=0)] \Delta v \rho_e[x_{e,k}(t=0)] \Delta x \\
&\quad \times \frac{1}{\sqrt{2\pi\varepsilon}} \exp\left\{-\frac{[x_i - x_{e,k}(t)]^2}{2\varepsilon^2}\right\}, \quad (23)
\end{aligned}$$

$$\begin{aligned}
R_h(x_i; t) &= \sum_k f_h[v_{h,k}(t=0)] \Delta v \rho_h[x_{h,k}(t=0)] \Delta x \\
&\quad \times \frac{1}{\sqrt{2\pi\varepsilon}} \exp\left\{-\frac{[x_i - x_{h,k}(t)]^2}{2\varepsilon^2}\right\}, \quad (24)
\end{aligned}$$

where ε is set at 2.5 times of the grid length Δx . Here, we assume for simplicity that each carrier density packet has a Gaussian distribution at each grid pixel in our finite element numerical approach.

The position and the velocity of the k th electron and hole can be calculated according to the Newtonian mechanics:

$$\begin{aligned}
\frac{dx_{e,k}}{dt} &= v_{e,k}, \\
\frac{dv_{e,k}}{dt} &= a(x_{e,k}), \quad (25)
\end{aligned}$$

$$\begin{aligned}
\frac{dx_{h,k}}{dt} &= v_{h,k}, \\
\frac{dv_{h,k}}{dt} &= a(x_{h,k}), \quad (26)
\end{aligned}$$

where the accelerations $a(x_{e,k})$ and $a(x_{h,k})$ were given in Eqs. (10) and (11). Equations (25) and (26) can be solved by the Runge-Kutta method for each time step to obtain $x_{e,k}(t)$, $x_{h,k}(t)$, $v_{e,k}(t)$, and $v_{h,k}(t)$. Because the charge density distribution of carriers $R(x_i; t)$ evolves in time as each carrier changes its position, these carrier density distributions need to be updated for each time step, which can be calculated by Eqs. (22)–(24). In our simulations, a time step of 50 fs was used to calculate the carrier trajectories at each time step and the evolution of the density maps.

III. RESULTS

Figure 2 shows the spatiotemporal evolution of the color-coded carrier density obtained by two different models on the $x - y$ plane at $t = 20$ ps. In Figs. 2(a)–2(d), taking the p -type region as an example, electrons originating from the p -type

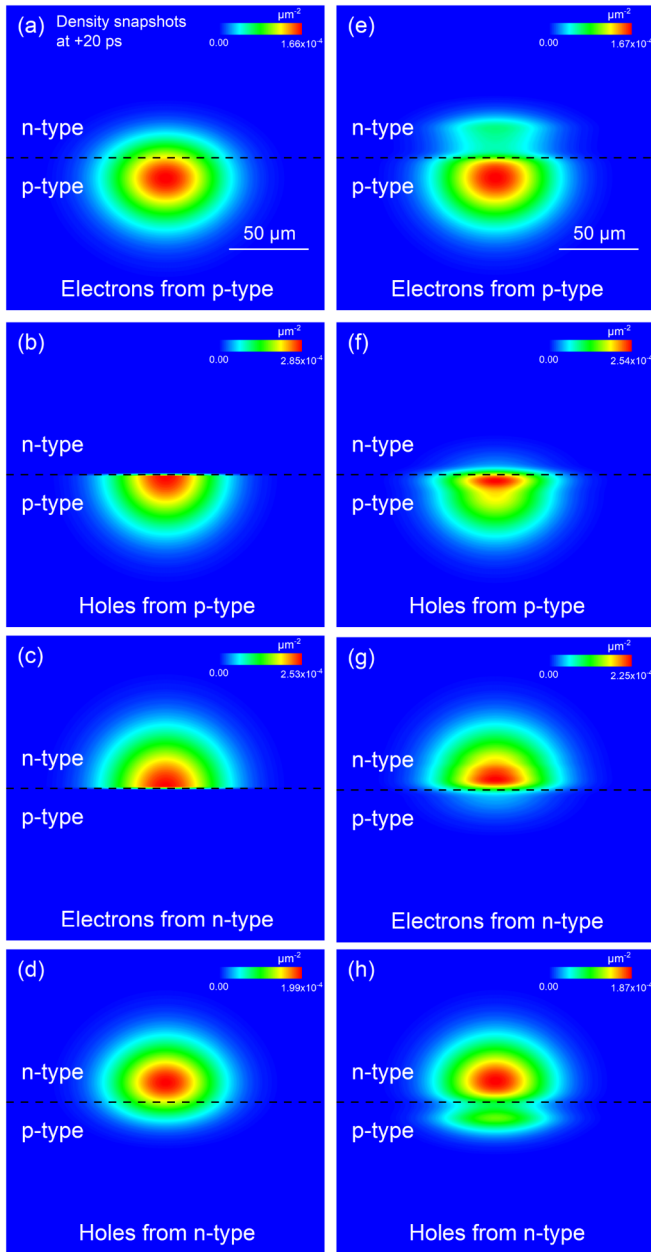


FIG. 2. Comparison of the carrier density maps at 20 ps after laser excitation based on simplified vs more realistic theoretical models. (a)–(d) Density distribution of electrons (red) and holes (blue) calculated by the simplified analytical model assuming a depletion zone with a straight vertical potential drop and assuming the kinetic energy of the electrons or holes is insufficient to climb over the potential wall (~ 1.12 eV). (e)–(h) Distributions of the carriers obtained by a more realistic model with an actual physical potential curve in the depletion zone and a more realistic Maxwell-Boltzmann velocity distribution of the carriers at high temperatures. Shown in (a) and (e) are the electron density maps for the initial electrons excited within the p -type region, whereas (b) and (f) show the hole density maps initially excited in the p -type region. Conversely, shown in (c) and (g) are the density maps for initial electrons excited within the n -type region, whereas (d) and (h) show the hole density maps initially excited in the n -type region. The effective mass and the mobility for electrons and holes are different.

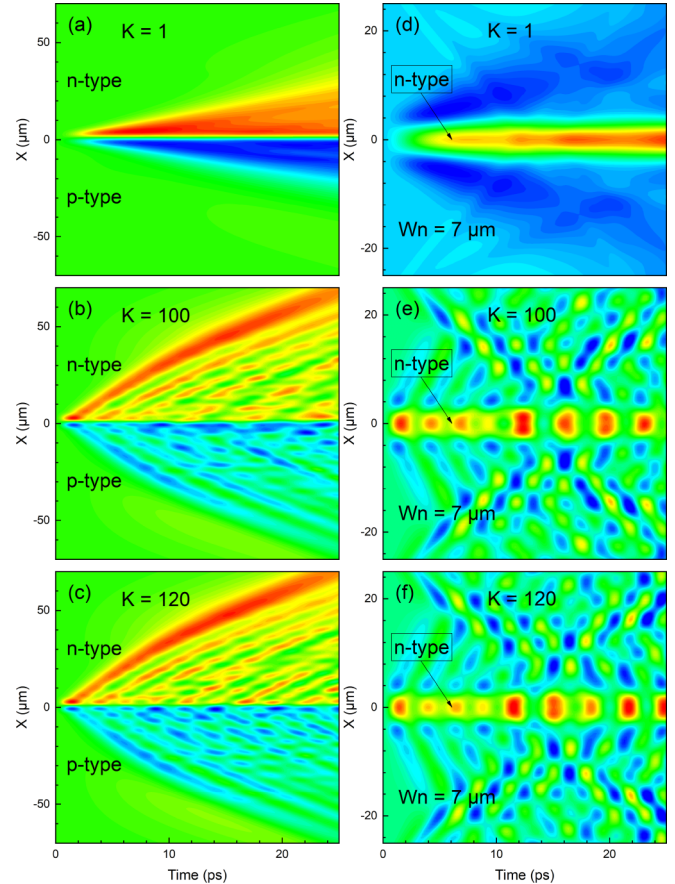


FIG. 3. Plasma waves in different multilayer semiconducting thin film junctions. Net charge density images reveal the plasma waves originating in the subplots (a)–(c) for a bipolar p - n junction and the subplots (d)–(f) for a p - n - p junction sandwiched by insulating layers. In the bipolar semiconductor, the net charge distribution for net electrons (red) and holes (blue) are present in the n - and p -type semiconductor regions, respectively. Quantum well-structured semiconductors possess superior performance in confining the movement of electrons and holes. The K value is directly proportional to the initial photoexcited number of electrons and holes in the semiconductor film structures. The parameter K is related to the Coulomb constant and the carrier density.

region will reach the n -type region. Conversely, according to the simplified model, the holes originating from the p -type region cannot climb over the barrier wall to reach the n -type region due to the vertical potential drop in the depletion zone. In Figs. 2(e) and 2(f), according to the more realistic model, electrons originating from the p -type region can be accelerated to reach the n -type region. Unlike the simplified analytical model, a small amount of highly energetic holes from the p -type semiconductor can reach the n -type region.

The above models, however, do not consider the Coulomb interactions among carriers. When the carrier density generated by a femtosecond laser excitation is sufficiently large, the Coulomb interactions must be included as done in our more realistic model. Figure 3 shows that the plasma wave phenomenon appears in the semiconductor junctions under the action of the inherent electric field in the depletion zone. The x -axis represents time, and the y -axis represents the distance

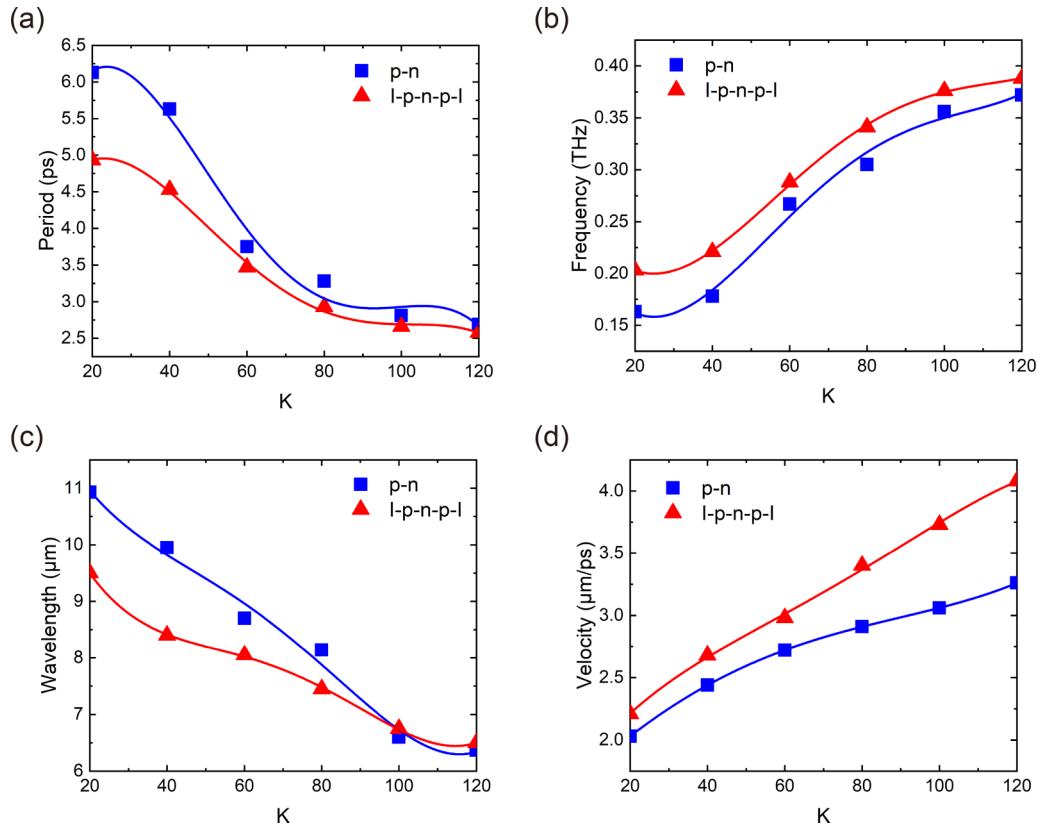


FIG. 4. Relevant parameters of plasma waves in two different semiconductor junctions. Shown are the corresponding calculated results for the (a) period, (b) frequency, (c) wavelength, and (d) wave front velocity. As the value of carrier density related parameter K increases, the frequency and wave front velocity of the plasma waves generated in the two types of semiconductors increase while the period decreases. The frequencies for these two types of plasma waves are in the subterahertz range, namely, between 0.18 and 0.37 THz.

from the center of the junction. The parameter K at 20, 40, 60, 80, 100, and 120 corresponds to an initial carrier number of 2.06×10^4 , 4.11×10^4 , 6.17×10^4 , 8.22×10^4 , 1.03×10^5 , and 1.23×10^5 in the 1D case, respectively. For the 2D case, the initial number of carriers is 4.23×10^8 , 1.69×10^9 , 3.80×10^9 , 6.76×10^9 , 1.06×10^{10} , and 1.52×10^{10} accordingly. The apparent echo phenomenon is observed in the structure of the $p-n-p$ junction sandwiched by an insulating layer. The insulator layers play an excellent role in confining the plasma wave propagation within the $p-n-p$ layers. In two different semiconductor junctions, peaks and troughs formed during the propagation of plasma waves are evident. When the K value or the laser intensity increases, propagation speed and oscillation prominence of the plasma wave also increase.

Figure 4 shows the dependencies of the period, frequency, wavelength, and propagation speed of the wave front of plasma waves on the parameter K (related to the carrier density). The calculated plasma wave frequency appears to be in the terahertz range, indicating that the EM radiation from such plasma oscillations also lies in the terahertz range.

IV. DISCUSSION

The purpose of this paper is to investigate the carrier dynamics in semiconductor junctions upon femtosecond laser excitation. In our previous experimental work using USEM to investigate carrier dynamics in a $p-n$ junction, we observed

a very fast appearance and ballistic expansion of the bright and dark SEM image domains on each side of the depletion zone, representing superfast transport of the hot electrons and holes. Here, we present a more realistic model to first explain such phenomena in a bipolar junction. Moreover, we predict the occurrence of plasma waves at high fluences. Owing to an increased density of photo-induced electrons and holes, the Coulomb interactions between the electron and hole clouds become so strong that they can result in charge density oscillations, thereby manifesting themselves as plasma waves. In this paper, we first utilized a simple model to describe the excitation of hot charged carriers and to simulate their ultrafast transport processes across a $p-n$ junction. Second, we extended and generalized this model to include the depletion zone potential curve and also the Coulomb interactions between the electron and hole clouds. Our analysis indicates that, at an increased carrier density with a high laser fluence, plasma oscillations can occur. We elucidate the plasma wave generation due to the rectification action by the intrinsic electric field in the depletion zone. On the one hand, the electric field causes the electron cloud to separate from the hole cloud, while on the other hand, the Coulomb attraction causes these two oppositely charged clouds to move toward each other. Such a push-and-pull action results in plasma oscillations near the junctions.

According to this paper, the photo-induced electron-hole cloud would expand rapidly, and because of the rectification

mechanism of the depletion zone at the p - n junction, hot electrons and holes would move differently to induce charge separation or rectification. At low laser fluence, bright and dark spots on either side of the junction in the USEM image were observed experimentally and reported by us and other coauthors. However, at a much higher fluence, we predict the appearance of plasma waves showing bright and dark fringes in the USEM image. Such plasma wave phenomena would become more prominent if we could increase the doping concentration of the p - n junction (well above 10^{19} cm $^{-3}$) or the fluence (well above 20 mJ/cm 2) so that the Coulomb attraction between the electron and hole clouds becomes more significant as the rise of plasma waves relies on the push-and-pull mechanism of two counterforces. As also predicted by this paper, such plasma wave phenomena would be more prominent if we could prepare a triode sandwiched by two insulating outlayers to confine the charge transport. Such USEM experiments would be quite interesting but challenging.

This paper is a purely theoretical work, presenting a more elaborated and realistic model as an extension of a simplified model used in our previous USEM work. The experimental conditions and basic simulation parameters used are similar in both works except that we consider here a p - n - p junction and a quantum well structure instead of a simple diode, and we also consider a high fluence regime. The maximum laser fluence used in the previous *Science* work [18] is 1.28 mJ/cm 2 , the estimated number of carriers is 10^9 , and the dopant concentrations for the p - and n -type semiconductors are 9.4×10^{18} cm $^{-3}$ and 1.4×10^{14} cm $^{-3}$, respectively. At such a low fluence, no plasma wave phenomena were observed. Therefore, one may need to increase the laser fluence or use samples with much higher impurity dopants for the p - and n -type semiconductors. We could not conduct any USEM experiments to observe the predicted plasma wave behavior at high laser fluence. The purpose of this paper is to arouse the interest among the USEM experimental teams to conduct such or other experiments.

Research on the ultrafast transport behavior of hot charge carriers could be extended in several directions. First, the photoexcitation of plasma waves in multilayer semiconducting junctions can be performed in future experiments. One could systematically simulate and analyze the plasma waves generated by various multilayer semiconductors, such as p - n and p - n - p junctions. The spatial extent of the plasma waves can be controlled by introducing two external insulating layers, and consequently, the intensity and duration of the plasma waves can be enhanced. Second, a terahertz detector could be used to measure the frequency and intensity

of EM radiation. Finally, the above semiconductor junctions are analyzed systematically to elucidate the key controlling factors of the frequency, wavelength, and power of such devices. We could use semiconductor films with a multilayer or multiquantum well structure to achieve a better design of a pulsed terahertz EM wave source based on photo-induced electron-hole plasma oscillations.

V. CONCLUSIONS

In summary, we investigated ultrafast photo-induced charge carrier dynamics in silicon junction structures. To analyze such dynamics, we employed a more realistic theoretical model that included Coulomb interactions among charged carriers and an actual depletion zone force field. These interactions played an important role when the carrier density was significantly high under strong laser excitation. The simulation results provided a qualitative explanation for the ultrafast charge separation and subsequent ballistic motion of electrons and holes across the p - n junction as reported in our previous experimental study [18]. Our simulations in this report here illustrated the underlying push-and-pull mechanism for the generation of plasma oscillations and wave propagation. Due to the shutdown of Zewail's lab after his unfortunate death, we could not resume the USEM experiments to test our predictions presented here. We hope such experiments could be conducted elsewhere by other groups. The wave frequency and velocity were found to increase with the carrier density, which was proportional to the laser fluence. Because these frequencies were in the terahertz range, such photo-induced electron-hole excitation and oscillation techniques in semiconductor junction structures could be potentially utilized as a means to generate pulsed terahertz EM radiation. Although terahertz radiation could also be generated in metals and semiconductors, our method using semiconductor junctions could provide better carrier confinement to enhance carrier density oscillations and also to affect the oscillatory behavior by applying an external direct current (DC) bias. The effects of a DC bias on the plasma wave behavior will be published elsewhere. Therefore, terahertz radiation generation by our method could be more flexibly controlled and effectively enhanced.

ACKNOWLEDGMENTS

This paper was supported by the National Natural Science Foundation of China (Grant No. 51727901, No. U1501241, and No. 11974264).

-
- [1] J. Ma, D. Kuciauskas, D. Albin, R. Bhattacharya, M. Reese, T. Barnes, J. V. Li, T. Gessert, and S. H. Wei, *Phys. Rev. Lett.* **111**, 067402 (2013).
 - [2] Y. C. Lin, W. C. Chou, A. S. Susha, S. V. Kershaw, and A. L. Rogach, *Nanoscale* **5**, 3400 (2013).
 - [3] D. Lagarde, L. Bouet, X. Marie, C. R. Zhu, B. L. Liu, T. Amand, P. H. Tan, and B. Urbaszek, *Phys. Rev. Lett.* **112**, 047401 (2014).
 - [4] Z. Zaaboub, F. Hassen, M. Naffouti, X. Marie, R. M'ghaieth, and H. Maaref, *Opt. Quantum Electron.* **49**, 142 (2017).
 - [5] S. Rawalekar, S. Kaniyankandy, S. Verma, and H. N. Ghosh, *J. Phys. Chem. C* **114**, 1460 (2010).
 - [6] M. Zürch, H. T. Chang, P. M. Kraus, S. K. Cushing, L. J. Borja, A. Gandman, C. J. Kaplan, M. H. Oh, J. S. Prell, D. Prendergast, C. D. Pemmaraju, D. M. Neumark, and S. R. Leone, *Struct. Dyn.* **4**, 044029 (2017).

- [7] L. Wang, Z. Wang, H. Y. Wang, G. Grinblat, Y. L. Huang, D. Wang, X. H. Ye, X. B. Li, Q. Bao, A. S. Wee, S. A. Maier, Q. D. Chen, M. L. Zhong, C. W. Qiu, and H. B. Sun, *Nat. Commun.* **8**, 13906 (2017).
- [8] P. Schiettecatte, P. Geiregat, and Z. Hens, *J. Phys. Chem. C* **123**, 10571 (2019).
- [9] S. Chouksey, P. K. Saha, V. Pendem, T. Aggarwal, A. Udai, S. Ganguly, and D. Saha, *Appl. Surf. Sci.* **518**, 146225 (2020).
- [10] E. M. Grumstrup, M. M. Gabriel, E. M. Cating, C. W. Pinion, J. D. Christesen, J. R. Kirschbrown, E. L. Vallorz, J. F. Cahoon, and J. M. Papanikolas, *J. Phys. Chem. C* **118**, 8634 (2014).
- [11] E. M. Van Goethem, C. W. Pinion, E. E. M. Cating, J. F. Cahoon, and J. M. Papanikolas, *ACS Photonics* **6**, 2213 (2019).
- [12] B. P. Mehl, J. R. Kirschbrown, R. L. House, and J. M. Papanikolas, *J. Phys. Chem. Lett.* **2**, 1777 (2011).
- [13] B. P. Mehl, J. R. Kirschbrown, M. M. Gabriel, R. L. House, and J. M. Papanikolas, *J. Phys. Chem. B* **117**, 4390 (2013).
- [14] E. S. Massaro, A. H. Hill, and E. M. Grumstrup, *ACS Photonics* **3**, 501 (2016).
- [15] E. M. Grumstrup, M. M. Gabriel, C. W. Pinion, J. K. Parker, J. F. Cahoon, and J. M. Papanikolas, *Nano Lett.* **14**, 6287 (2014).
- [16] M. M. Gabriel, J. R. Kirschbrown, J. D. Christesen, C. W. Pinion, D. F. Zigler, E. M. Grumstrup, B. P. Mehl, E. E. M. Cating, J. F. Cahoon, and J. M. Papanikolas, *Nano Lett.* **13**, 1336 (2013).
- [17] D. S. Yang, O. F. Mohammed, and A. H. Zewail, *Proc. Natl Acad. Sci. USA* **107**, 14993 (2010).
- [18] E. Najafi, T. D. Scarborough, J. Tang, and A. Zewail, *Science* **347**, 164 (2015).
- [19] R. Bose, J. Sun, J. I. Khan, B. S. Shaheen, A. Adhikari, T. K. Ng, V. M. Burlakov, M. R. Parida, D. Priante, and A. Goriely, *Adv. Mater.* **28**, 5106 (2016).
- [20] B. Liao, E. Najafi, H. Li, A. J. Minnich, and A. H. Zewail, *Nat. Nanotechnol.* **12**, 871 (2017).
- [21] E. Najafi, V. Ivanov, A. Zewail, and M. Bernardi, *Nat. Commun.* **8**, 15177 (2017).
- [22] C. Jacoboni and L. Reggiani, *Rev. Mod. Phys.* **55**, 645 (1983).
- [23] M. Bernardi, D. Vigil-Fowler, C. S. Ong, J. B. Neaton, and S. G. Louie, *Proc. Natl. Acad. Sci.* **112**, 5291 (2015).
- [24] G. D. Tsibidis, L. Mouchliadis, M. Pedio, and E. Stratakis, *Phys. Rev. B* **101**, 075207 (2020).
- [25] M. V. Exter, C. Fattinger, and D. Grischkowsky, *Appl. Phys. Lett.* **55**, 337 (1989).
- [26] P. Gu, M. Tani, S. Kono, K. Sakai, and X. C. Zhang, *J. Appl. Phys.* **91**, 5533 (2002).
- [27] A. G. Davies, E. H. Linfield, and M. B. Johnston, *Phys. Med. Biol.* **47**, 3679 (2002).
- [28] D. Dragoman and M. Dragoman, *Prog. Quantum Electron.* **28**, 1 (2004).
- [29] J. Lutz, H. Schlangenotto, U. Scheuermann, and R. D. Doncker, *Semiconductor Power Devices* (Springer, Berlin, Heidelberg, 2011).